ANALYSIS OF THE INFLUENCE OF THE SOFT-SWITCHING IN THE SMALL-SIGNAL MODEL OF THE ZVS-PSM-FB DC-DC CONVERTER

Cleber Zanatta, José Renes Pinheiro
Federal University of Santa Maria – UFSM, Power Electronics and Control Research Group - GEPOC
Av. Roraima, n°1000, CEP 97105-900, Santa Maria, RS - Brazil
http://www.ufsm.br/gepoc, cleberzanattak@gmail.com, renes@ctlab.ufsm.br

***Abstract* – In this work it is investigated the possibility to extend ZVS-PSM-FB small signal dynamic model presented in [6] to the ZVS-PSM-FB with two auxiliary commutation circuits since both converters are similar. At first, it is re-evaluated the small signal model parameters for the purpose of matching with each converter characteristics. The main contribution of this paper is to take into consideration the soft-switching action effects on steady-state operation and the small-signal model of the ZVS-PSM-FB family converters. Experimental and theoretical frequency response results of both converters show a good matching between them.**

***Keywords* – Full-Bridge ZVS, Phase-Shift Modulated, Small-signal model, CC-CC Converter, Telecom power Supplies.**

I. INTRODUCTION

The zero-voltage-switching phase-shift-modulated full-bridge (ZVS-PSM-FB) buck-type dc-dc converter has been an attractive topology for high-power rectifiers for telecommunications and distributed power systems [1-3, 6-8]. This converter has ZVS on all active switches using intrinsic parasitics components. This soft-switching action enables the converter to operate in reduced switching losses and stresses, eliminating the need for primary snubbers.

The operation of this converter is characterized by an interval of loss of duty-cycle that decreases the control action at the secondary of the converter. This interval has a non-linear characteristic, being dependent on converter operation point and components values. This non-linearity complicates the analysis of both steady-state and small-signal dynamics.

Previous works [2-6] have derived equations for steady-state and small-signal dynamics for this converter. In [2], a simple s-domain polynomial ratio transfer function was derived. But this approach was based on the buck small-signal model, and its derivation is not formal and the steady-state equations are defective.

In [3], a more rigorous mathematical development is presented, but the resulted dynamical model is a complex maze of feedback blocks diagram. Despites its good match between experimental and theoretical results of the input-to-output transfer function, the same success cannot be achieved to the control-to-output transfer function, that is used to design the converter control loop.

In [4-6] were developed two simple s-domain polynomial ratio transfer function small-signal dynamical models for the ZVS-PSM-FB, where the dynamical model derived in [5-6] was able to overcome the drawbacks of the previous model [4], being simple and approximate model for the ZVS-PSM-FB converter.

Despite the advantages of the ZVS-PSM-FB converter, the range of ZVS operation of this converter is restricted from full-load down to some amount of load defined by the design. The ZVS range is limited by the size of parasitics components and the resonant inductance L_R, being not desirable to increase this inductance value since it will also increase the loss of duty cycle interval.

To overcome this limitation, the zero-voltage-switching phase-shift-modulated full-bridge with two auxiliary commutation circuits (ZVS-PSM-FB-2ACC) was presented in [7], where the two auxiliary circuits are used to extend the soft-switching range from full to zero load.

This converter is also attractive for high power applications since the desirable extension of the ZVS range and the reduced switching losses comes with a low increase in its cost.

In this work, it will be analyzed the possibility to extend the ZVS-PSM-FB converter dynamical model for the ZVS-PSM-FB-2ACC converter. At first, it will be performed a ZVS-PSM-FB converter dynamical model parameters re-evaluation. Then the parameters will be adjusted to the ZVS-PSM-FB-2ACC to develop a small-signal dynamic model for this converter.

Experimental frequency response results of a 48V/12.5A converter, of both topologies, shown and compared with theoretical results.

II. ZVS-PSM-FB DC-DC CONVERTERS

In this section will be shown both ZVS-PSM-FB and ZVS-PSM-FB-2ACC DC-DC converters, theirs circuits, waveforms and main features.

A. The ZVS-PSM-FB Converter

The ZVS-PSM-FB topology is shown on Fig. 1, and its CCM steady-state operation waveforms on Fig. 2. During stages 6 and 7 the control action is applied to the active switches on primary side of the converter, but at the secondary, the rectifiers are still short-circuited. These stages time intervals are known as loss of duty cycle ΔD, who is non-linear and dependent on converter operation point what difficult the analysis of converter dynamics and steady-state operation.

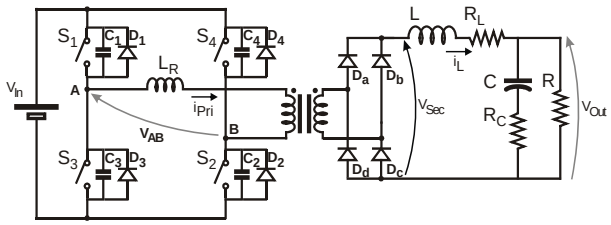

Fig. 1. ZVS-PSM-FB DC-DC Converter circuit schematics.

Despites its buck characteristics, both the steady-state and dynamics characteristics of the ZVS-PSM-FB must take into account the loss of duty cycle effect to correctly model its behaviours.

In [5-6], it is shown approximate steady-state equations for the control duty-cycle D and loss of duty-cycle ΔD, expressed by:

$$D = \frac{V_{Out}}{nV_{In}}\left(1+\Delta D\frac{n^2L_R}{L}\right)+\Delta D \quad (1)$$

and

$$a\Delta D^2 + b\Delta D + c = 0 \quad (2)$$

where

$$a = \frac{n^2L_R}{L}\left(1+\frac{V_{Out}}{nV_{In}}\frac{n^2L_R}{L}\right)$$

$$b = 1+\frac{n^2L_R}{L}\left(2\frac{V_{Out}}{nV_{In}}-1\right)-\frac{nV_{In}}{V_{Out}}\left(\frac{L}{n^2L_R}+1\right)$$

$$c = \frac{V_{Out}}{nV_{In}}+4f_s\frac{\left(L+n^2L_R\right)}{R}-1$$

The loss of duty cycle interval ΔD and the range of ZVS are proportional to the value of the resonant inductance L_R. The wider the desired ZVS operation range the higher the resonant inductance value and thus the greater the loss of duty cycle interval. A proper design of this converter needs to deal with these features, in order to maximize the ZVS range without penalize the control action and the transformer manufacturing.

The left leg switches commutations are less problematic since the converter output load is used to perform the commutation. The right leg switches commutations occurs when the transformer is short-circuited, being only available the energy stored at the primary parasitic components to perform this commutation.

With the steady-state equations (1) and (2), and the AC Equivalent Circuit Small-Signal Modelling Technique, presented in [8], two simple polynomial ratio form transfer-function small-signal model were derived on [3-5], where were able to closely model the ZVS-PSM-FB converter dynamics.

The key point of small-signal model development is know how the ratio between a positive output current i_L small perturbation and the loss of duty cycle was derived, as shown in Fig. 3. Also, there is the important substitution of the loss of duty cycle perturbed variable $\Delta\hat{d}$, by a sum of the inputs, v_{In}, i_L and d, and output, v_{Out}, perturbed variables effects over the loss of duty cycle interval.

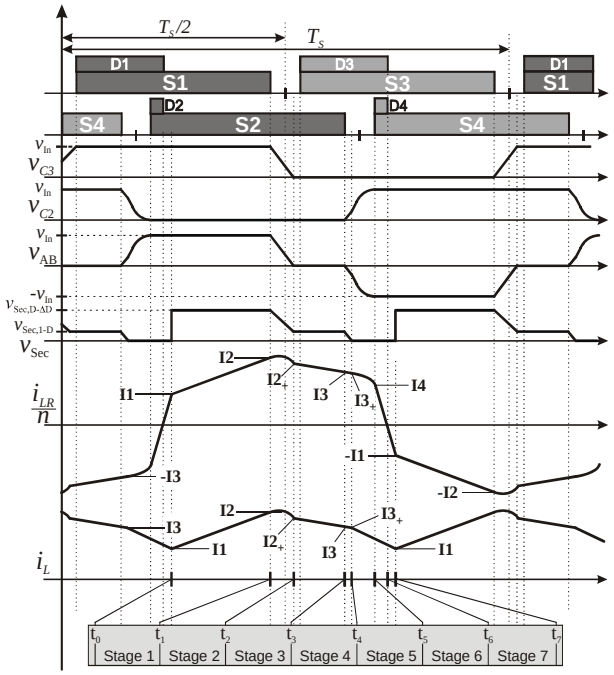

Fig. 2. Steady-State operation converter waveforms.

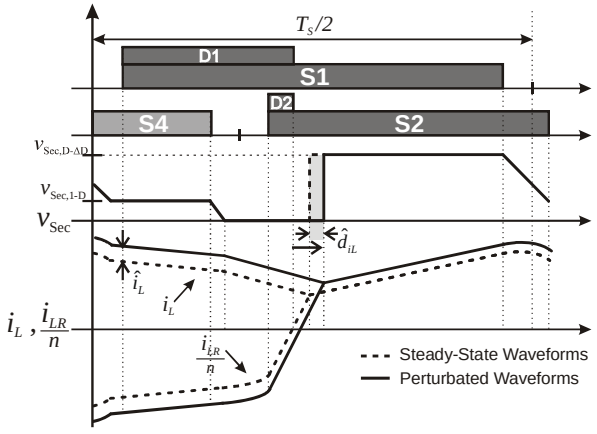

Fig. 3. ΔD perturbation due to a positive i_L perturbation.

This ratio of a positive output current perturbation and the loss of duty cycle interval will be analysed on the next section, since there are many approaches to it.

B. The ZVS-PSM-FB-2ACC Converter

This converter was developed to extend the range of ZVS from full to zero load. The loss of duty cycle is reduced since most part of the energy used to perform the switches commutations come from the auxiliary circuit and so, there is no need to have a high resonant inductance value at the primary to achieve a desired ZVS load range

The ZVS-PSM-FB-2ACC circuit schematic is shown on Fig. 4 and its steady-state CCM operation waveforms on Fig. 5. The input voltage source is split in two, where between it and the central point of the legs are connected two auxiliary inductors, L_1 and L_2.

As the resonant inductor value is smaller, the loss of duty cycle has less influence in the control action, but this effect is not eliminated in this converter.

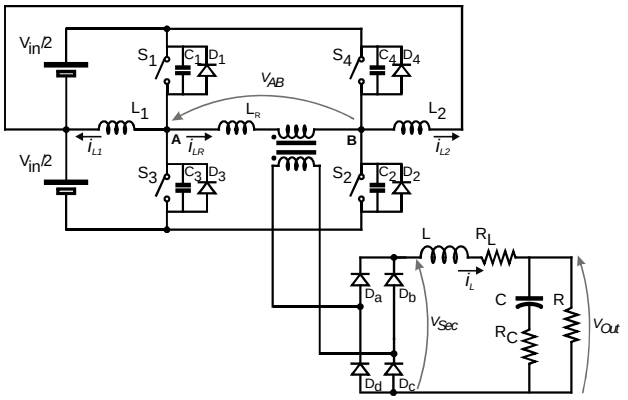

Fig. 4 . ZVS-PSM-FB-2ACC DC-DC Converter circuit schematics.

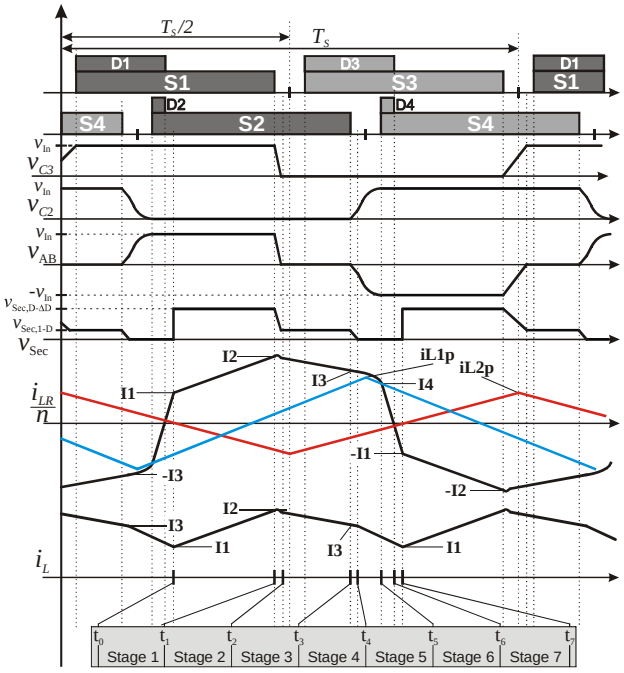

Fig. 5. ZVS-PSM-FB-2ACC Steady-State converter operation waveforms.

Quiescent point of operation can also be approximately determined by equations (1) and (2) of the previous converter.

Since operations of both converters are similar, the use of the same dynamic model and steady-state equations is a natural attempt. In the next section, the dynamic model parameters are matched with converter characteristics, and thus, obtaining the dynamical model for each converter.

III. SMALL-SIGNAL MODEL PARAMETERS IMPROVEMENT

A. Loss of Duty-Cycle Effect Equivalent Impedance - $Z_{\Delta d}$

During the small-signal dynamical model development of the ZVS-PSM-FB [2-5], and ZVS-PSM-FB-2ACC converters, it was necessary to substitute the perturbed loss of duty cycle variable $\Delta\hat{d}$ by a sum of equivalent equations proportional to the suitable variables (v_{In}, v_{Out}, i_L and d) used for conventional converters dynamics analysis.

Development of an equivalent equation relating the effect of an output current positive perturbation $\hat{i}_L$ over the loss of duty cycle interval, takes into account the stages equations and waveforms geometry, as shown on Fig. 3. The resulting equation has a resistive characteristic when applied back to the models, i.e., representing a decrease of the converter gain, due the loss of duty cycle interval.

On [2] and [3], the resonant stages 4 and 5, Fig. 3, are not considered into the development of the equivalent equation. The resulted equivalent impedance $Z_{\Delta d}$ is constant over the entire load range, meaning that the loss of duty cycle has always the same effect in the dynamics of the converter, and are given by:

$$Z_{\Delta D,\ from[2]\ and[3]} = 4n^2 L_R f_s \qquad (3)$$

On [4], it is shown that the resonant stage previous the loss of duty cycle interval has an important role in the characterization of the equivalent impedance $Z_{\Delta d}$. In this approach, the impedance $Z_{\Delta d}$ is a function of the load.

$$Z_{\Delta d,\ from[4]} = 2\left(1+\cos\left(\omega_5 t_{E5}\right)\right) n^2 L_R f_s \qquad (4)$$

On [5], stages 4 and 5 are also not considered, but the approximate equivalent impedance $Z_{\Delta d}$ equation is a function of the load by means of the loss of duty cycle variable ΔD.

$$Z_{\Delta d,\ from[5]} = \Delta D_{(2)}.R\frac{nV_{In}}{V_{Out}}\left(1+\frac{n^2 L_R}{L}\frac{V_{Out}}{nV_{In}}\right) \qquad (5)$$

Since there are many approaches to the loss of duty cycle effect on the dynamical model of the converter, simulation of the resulting effect of a positive output current perturbation over the loss of duty-cycle of both converters was performed, and the results are shown in Fig. 6 and Fig. 7, using the design parameters from Table 1 and 2. The simulation results are compared with the equivalent impedance $Z_{\Delta d}$ equations (3-5).

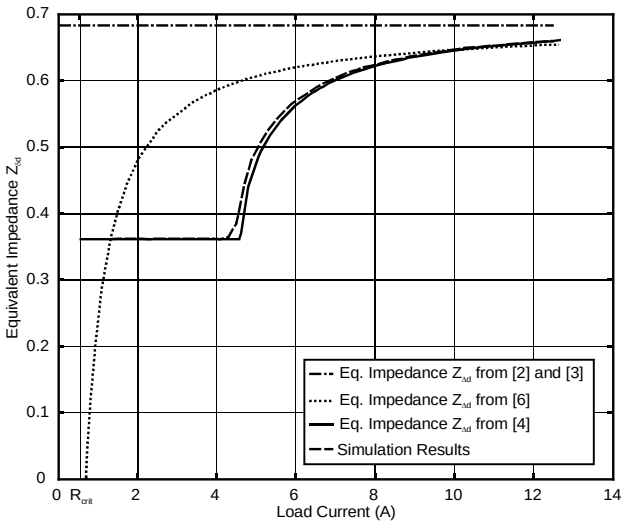

Fig. 6. ZVS-PSM-FB loss of duty-cycle equivalent impedance $Z_{\Delta d}$ comparison.

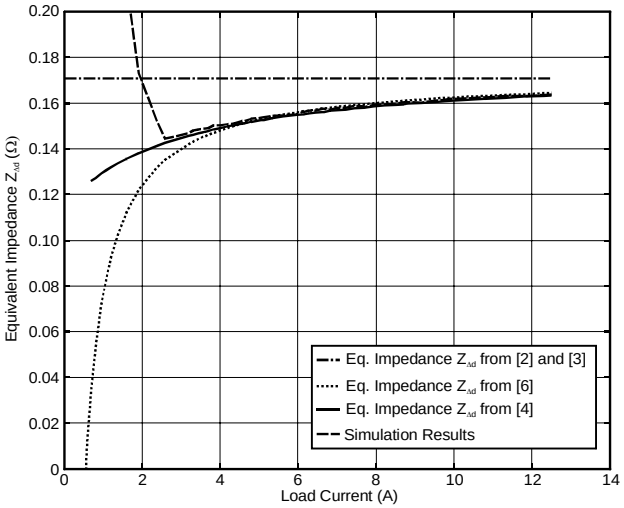

Fig. 7 – ZVS-PSM-FB-2ACC loss of duty-cycle equivalent impedance $Z_{\Delta d}$ comparison.

From Fig. 6, it can be seen that the equation (4) equivalent impedance $Z_{\Delta d}$ developed in [4] is the closer result from that obtained in simulation (continuous line). From Fig. 7, it can be seen that equation (4) agrees with the simulation from full-load to about 20% of load. The sudden change of the $Z_{\Delta D}$ in Fig. 7 is a result of the absence of stages 6 and 7 (as shown on Fig. 9b waveforms 4 and 5) during the loss of duty cycle interval. For the above demonstrated, equation (4) can model the loss of duty cycle equivalent impedance $Z_{\Delta D}$ in all ZVS-PSM-FB load range and about 20% to full load ZVS-PSM-FB-2ACC converter.

Table 1
ZVS-PSM-FB Prototype Converter Parameters

Input Voltage, V_{In}	360V	Output Voltage, V_{Out}	48V
Resonant Inductance, L_R	40µH	Output Inductance, L	76µH
Switching Frequency, f_s	100kHz	Output Capacitance, C	220µF
Capacitor ESR, R_C	32mΩ	Output Inductance ESR, R_L	15mΩ
Transf. turns ratio n_2/n_1, n	1/4.84	Output Load range, I_{Out}	0 - 12.5A

B. Control Duty-Cycle and Loss of Duty-Cycle Equation

Derivation of equations (1) and (2) in [3] and [5] do not take into account the resonant stages. Despite the acceptable accuracy, the dynamical model present in [4] do not present satisfactory transfer functions dc-gains response over the load range, as reported in [6].

Following the same procedure used to derive the loss of duty cycle presented in [3], but now taking the resonant stages 4 and 5 into account, it is possible to demonstrate that the loss of duty cycle ΔD, can be expressed as:

$$\Delta D = \Delta D_{(2)} - \delta D_{t_5} + t_{E5} \,/\, T_S \qquad (6)$$

Where, $\Delta D_{(2)}$ is the same result obtained from equation (2) and δD_{t5} is given by:

$$\delta D_{t_5} = \frac{2 f_s n^2 L_R}{n V_{In}} \left[I_3 \left(1 - \cos\left(\omega_5 t_{E5}\right)\right) + \frac{V_{C2}\left(t_4\right)}{n Z_5} \sin\left(\omega_5 t_{E5}\right) \right] \qquad (7)$$

where t_{E5} is the total time of stage 5, ω_5 and Z_5 are functions of L_R and $2*C_{Switch}$.

On Fig. 8b the equation (6), (2) and CAD-simulated results are plotted, where can be seen that simulation results and equation (6) agree very closely all over the load range. Also on Fig. 8b, the simulated time interval of stages 6 and 7 and the result from equation (6) are plotted, and they agree very closely.

To develop the control duty-cycle equation, it will also be taking into account the resonant stages, and following the same procedure demonstrated in [3] and [5], it is possible to demonstrate that the control duty cycle D is given by:

$$D = \frac{V_{Out}}{n V_{In}} \left(1 + R_L \,/\, R\right) \left(1 + \Delta D \frac{n^2 L_R}{L}\right) + \Delta D - \frac{1}{2} t_{E2} \frac{2}{T_s} \qquad (8)$$

Where t_{E2} and t_{E5} are the time duration of stages 2 and 5 respectively, and they are expressed by:

$$t_{E2} = \frac{1}{\omega_2} \left[\operatorname{asin}\left(\frac{V_{Out}/n}{\sqrt{\left(V_{Out}/n - V_{In}\right)^2 + \left(\frac{Z_2 I_2}{n}\right)^2}} \right) - \operatorname{atg}\left(\frac{\left(V_{Out}/n - V_{In}\right)}{\frac{Z_2 I_2}{n}} \right) \right] \qquad (9)$$

where ω_2 and Z_2 are functions of $(L+n^2L_R)$ and $2C_{Switch}/n^2$ and

$$t_{E5} = \frac{1}{\omega_5} \left[\operatorname{asin}\left(\frac{V_{In}}{\sqrt{\left(n Z_5 I_3\right)^2 + \left(V_{C2}\left(t_4\right)\right)^2}} \right) - \operatorname{atg}\left(\frac{V_{C2}\left(t_4\right)}{n Z_5 I_3} \right) \right] \qquad (10)$$

On Fig. 8a all the three functions are similar, but the equation (8) is the only function that follows the CAD-simulated results.

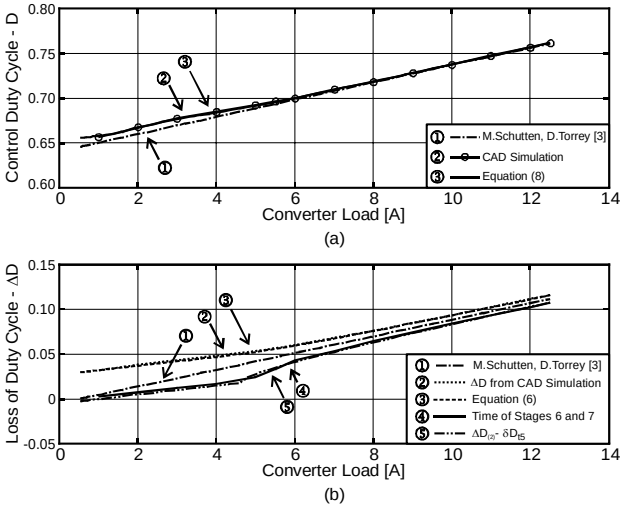

Fig. 8. ZVS-PSM-FB with design parameters from Table 1 (a) control duty-cycle comparison. (b) loss of duty-cycle comparison.

The above derived equations demonstrate that despites the soft-switching stages intervals are short in this converter, the evolution of the variables, involved both in circuit operation and in the soft-switching, they have an important role of fine tuning the equations that determine the quiescent point of converter operation.

For the ZVS-PSM-FB-2ACC converter, shown on Fig. 4, the auxiliary circuits added to help the soft-switching action, results in a meaningful reduction of soft-switching effects over the converter waveforms. Equations (6) and (8) can also obtain the steady-state quiescent point of operation, however equations (7), (9) and (10) must be substituted by respectively:

$$\delta Dt_5 = \frac{2 f_s n^2 L_R}{n V_{In}} \left[\left(I_3 + \frac{I_{L2p}}{n} \right) \left(1 - \cos\left(\omega_5 t_{E5}\right)\right) + \frac{V_{C2}(t_4)}{n Z_5} \sin\left(\omega_5 t_{E5}\right) \right] \quad (11)$$

$$t_{E2} = \frac{1}{\omega_2} \left[\operatorname{asin}\left(\frac{\frac{V_{Out}}{n}}{\sqrt{\left(\frac{V_{Out}}{n} - V_{In}\right)^2 + \left[\frac{Z_2}{n}\left(I_2 + \frac{I_{L1p}}{n}\right)\right]^2}} \right) - \operatorname{atg}\left(\frac{\left(\frac{V_{Out}}{n} - V_{In}\right)}{\frac{Z_2}{n}\left(I_2 + \frac{I_{L1p}}{n}\right)} \right) \right] \quad (12)$$

and

$$t_{E5} = \frac{1}{\omega_5} \left[\operatorname{asin}\left(\frac{V_{In}}{\sqrt{\left[Z_5\left(nI_3 + I_{L2p}\right)\right]^2 + \left(V_{C2}(t_4)\right)^2}} \right) - \operatorname{atg}\left(\frac{V_{C2}(t_4)}{Z_5\left(nI_3 + I_{L2p}\right)} \right) \right] \quad (13)$$

where I_{L2p} is the peak current value of auxiliary inductor *L2*.

On Fig. 9a, it is shown the comparison of equation (1) with CAD-simulation, where can be seen that the soft-switching, helped by the auxiliary circuits, have less effect on determination of converter quiescent point of operation.

On Fig. 9b, is shown the comparison of equation (6) with CAD-simulated data. For the simulation results obtained, the curves presents a well behaviour fashion, seemed that the soft-switching is not modifying too much the waveforms.

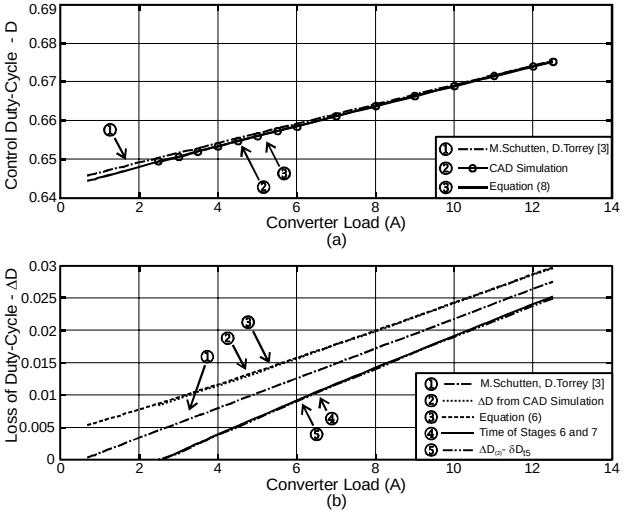

Fig. 9. ZVS-PSM-FB-2ACC (a) Control Duty-Cycle Comparison. (b) Loss of Duty-Cycle Comparison.

Table 2
ZVS-PSM-FB-2ACC Prototype Converter Parameters

Input Voltage, V_{In}	360V	Output Voltage, V_{Out}	48V
Resonant Inductance, L_R	10µH	Output Inductance, L	76µH
Auxiliary Inductance 1, L_1	345µH	Auxiliary Inductance 2, L_2	210µH
Switching Frequency, f_s	100kHz	Output Capacitance, C	220µF
Capacitor ESR, R_C	32mΩ	Output Inductance ESR, R_L	15mΩ
Transf. turns ratio n_2/n_1, n	1/4.84	Output Load range, I_{Out}	0-12.5A

IV. ZVS-PSM-FB AND ZVS-PSM-FB-2ACC SMALL SIGNAL MODEL

Using the AC equivalent circuit small-signal modelling technique, presented in [8], it was derived the small signal model for both converters. For both converters, the input-to-output G_{vg}, and control-to-output G_{vd} transfer functions have the same form and they are given by:

$$G_{vg}(s) = \frac{n\left[D + \left(\frac{1}{2}t_2 - t_5\right)\frac{2}{T_s}\right](sCR_C + 1)}{As^2 + Bs + E} \quad (14)$$

$$G_{vd}(s) = \frac{nV_{In}(sCR_C + 1)}{As^2 + Bs + E} \quad (15)$$

where

$$A = \left(L + n^2 L_R\right) C \left(1 + \frac{R_C}{R}\right)$$

$$B = \left\{ \begin{array}{l} \left(L + n^2 L_R\right) + C\left(R + R_C\right)\left(R_L + Z_{\Delta d} + \Delta D \frac{n^2 L_R}{L} R_L \right) + \\ + CR\left(R_C + t_2 \frac{2}{T_S} \frac{n^2 L_R}{L} R_L \right) \end{array} \right\} \frac{1}{R}$$

$$E = 1 + \left(R_L + Z_{\Delta d} + \Delta D \frac{n^2 L_R}{L} R_L \right) \frac{1}{R}$$

and $Z_{\Delta d}$, D and ΔD are given by equations (4), (8) and (6).

V. EXPERIMENTAL RESULTS

A 600W ZVS-PSM-FB converter prototype, with design parameters given in Table 1, was built in order to compare the experimental measurements from Input-to-Output and Control-to-Output transfer functions. The equipment used to perform the measurements is an AP200 from Ridley Engineering [9].

On Fig. 10 and 11, experimental results are compared with the frequency response of equation (14) for input-to-output and equation (15) for control-to-output.

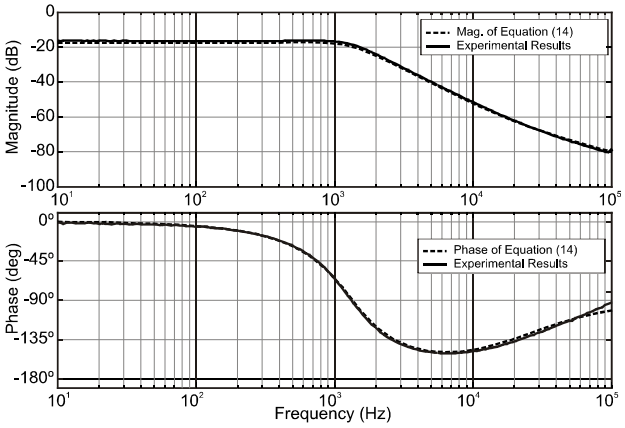

Fig. 10. ZVS-PSM-FB Input-to-Output transfer function experimental results and theoretical predictions.

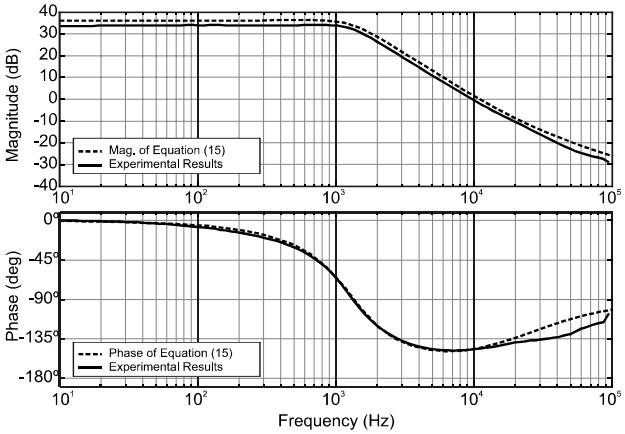

Fig. 11. ZVS-PSM-FB Control-to-Output transfer function experimental results and theoretical predictions.

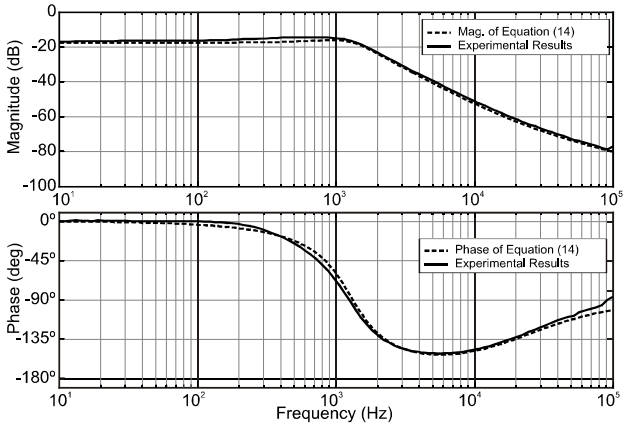

Fig. 12 ZVS-PSM-FB-2ACC Input-to-Output transfer function experimental results and theoretical predictions.

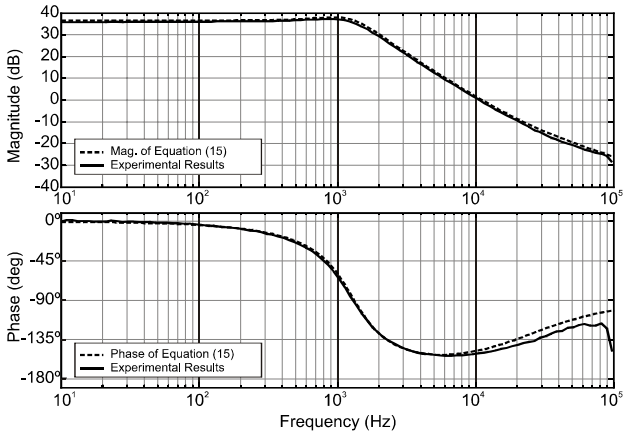

Fig. 13 ZVS-PSM-FB-2ACC Control-to-Output transfer function experimental results and theoretical predictions.

Experimental results of a 600W ZVS-PSM-FB-2ACC input-to-output and control-to-output transfer functions, with converter parameters from Table 2, are shown on Fig. 12 and Fig. 13 and compared with equations (14) and (15).

Comparison of the experimental results and theoretical predictions shows a good matching of the frequency responses for both converters. Small divergence between experimental and theoretical can be explained by component value variations due frequency and manufacturing.

VI. CONCLUSIONS

In this work it was presented a new small-signal model of the ZVS-PSM-FB resulted due a re-evaluation in converter model parameters and steady-state equations of control duty cycle and loss of duty cycle.

It was also extended this new small-signal model to the ZVS-PSM-FB-2ACC, that is a similar converter to the ZVS-PSM-FB, but it has two auxiliary commutation circuits to help the ZVS action of the switches for all over the load range.

The derived parameters equations are almost the same for both converters, being different only in some specifically characteristics of each converter, and it was demonstrated what are this differences to avoid misuse of them when applying in one of the converters dynamical model.

Experimental results of both converters have shown a good match with theoretical results for both input-to-output and control-to-output transfer functions, showing its worthwhile theoretical dynamical modeling effort.

REFERENCES

[1] J. A. Sabatè, V. Vlatkovic, R. B. Ridley, and F. C. Lee, “Design considerations for high-voltage high-power full-bridge zero-voltage-switched PWM converter”, in *Proc. IEEE APEC’90 Conf.*, pp. 100-110, 1988.

[2] V. Vlatkovic, J.A. Sabatè, R.B.Ridley, F.C. Lee, and B.H.Cho,”Small-signal analysis of the phase-shifted PWM converter”, in IEEE Transactions on Power Electronics”, Vol. 7, No 1, pp.128-135, Jan 1992.

[3] M. Schutten and D. A. Torrey, “Improved small-signal analysis for the phase-shifted PWM power converter,” in IEEE Transactions on Power Electronics, Vol. 18, No 2, pp.659-669, March,2003.

[4] C. Zanatta and J. R. Pinheiro, “A new small-signal model for the ZVS-phase-shift-modulated full-bridge DC-DC converter”, in 7th *International Conference on Industrial Applications* INDUSCON’2006, Recife, PE, Brazil, April 2006.

[5] C. Zanatta and J. R. Pinheiro, “Modelo de pequenos sinais do conversor CC-CC ponte-completa com modulação por deslocamento de fase e comutado sob zero de tensão (ZVS-PSM-FB) com erro nulo de ganho-CC”, in 14th Brazilian Conference on Automatics, CBA 2006, Salvador, BA, Brazil, Oct. 2006.

[6] C. Zanatta and J. R. Pinheiro, “A no dc-gain error small-signal model for the zero-voltage-switching phase-shift-modulated full-bridge dc-dc converter”, in 32nd IECON, Paris, Nov. 2006.

[7] J. L. F Vieira, “Concepção, análise e projeto de sistemas de alimentação em corrente contínua de alto desempenho com altas freqüência e potência", Doctorate Thesis, UFSC, Brazil, March. 1993;

[8] R. W. Erickson and D. Maksimovic, *Fundamentals of Power Electronics*, 2nd Edition, Kluwer Academics, 2001.

[9] AP200 – *Frequency Response Analyzer* – AP Instruments Inc. *http://www.apinstruments.com* and Ridley Engineering Inc. – *http://www.ridleyengineering.com.*